Ocean Engineering 292 (2024) 116538

Contents lists available at ScienceDirect

Ocean Engineering

journal homepage: www.elsevier.com/locate/oceaneng

Distributions and extreme value analysis of critical response rate and split-time metric in nonlinear oscillators with stochastic excitation

Dylan Glotzer [a], Vladas Pipiras [b,*], Vadim Belenky [c], Kenneth M. Weems [c], Themistoklis P. Sapsis [d]

[a] Mathematics and Computer Science Department, Science and Math Building, Meredith College, Raleigh, NC 27607, USA
[b] University of North Carolina, USA
[c] Naval Surface Warfare Center Carderock Division (NSWCCD), 9500 MacArthur Blvd, W. Bethesda, MD 20817, USA
[d] Department of Mechanical Engineering, Massachusetts Institute of Technology, 77 Massachusetts Ave., Cambridge, MA 02139, USA

ARTICLE INFO

Keywords:
Nonlinear oscillator
Stochastic excitation
Softening restoring
Split-time method
Extreme value theory
Peaks over threshold

ABSTRACT

A single-degree-of-freedom oscillator with a nonlinear restoring force and stochastic external forcing is studied with the goal of understanding the distributions of certain response rates. Motivated by applications to ship motions, the response rates concern the minimum response rate leading to capsizing (the critical response rate) and a measurement comparing an observed response rate to the critical response rate (the split-time metric), whose distributions are investigated both analytically and numerically. Three nonlinear restoring forces are considered: piecewise linear (experiencing linearly softening stiffness above a "knuckle" point), doubly piecewise linear (experiencing piecewise linearly softening stiffness above a "knuckle" point), and the cubic softening restoring force of the Duffing oscillator. In the first two cases, an efficient numerical simulation of the critical response rate and split-time metric is proposed from a derived distribution; in the latter case, the density of the critical response rate is approximated assuming white noise excitation. A key interest is in the nature of the right tail of the split-time metric, specifically as it relates to its extrapolation through extreme value analysis in estimating the probability of capsizing. The distribution is found to have a "light" tail, which motivates the use of exponential rather than the generalized Pareto distribution for exceedances above threshold in extreme value analysis. Finally, threshold selection through a prediction error criterion for the exponential distribution is examined, and the Weibull distribution tail is suggested as a useful means for a more refined examination of the distribution tail.

1. Introduction

The focus of this work is on certain questions related to a single-degree-of-freedom nonlinear oscillator given by

$$\ddot{x}(t) + 2\delta\dot{x}(t) + r(x(t)) = y(t), \tag{1.1}$$

with a softening restoring force (stiffness) $r(x)$ that is characterized by an unstable equilibrium, as e.g. in the special cases of piecewise linear restoring forces depicted in Fig. 1. In (1.1), $\delta > 0$ is a damping parameter and $y(t)$ is an external stochastic excitation (forcing). Both suitable correlated and white noise excitations will be considered below.

Nonlinear oscillators (1.1), with both stochastic and deterministic excitation, play a central role in a wide range of areas and applications, as canonical models for oscillatory phenomena. See e.g. Nayfeh and Mook (2008), Belenky and Sevastianov (2007), or Hayashi (2014). Our primary interest behind (1.1) relates to its use as a prototypical qualitative model of roll motion of a ship in irregular (random) beam seas. The model (1.1) incorporates the possibility of capsizing, understood as the transition through the unstable equilibrium (for example, towards another stable equilibrium or to diverge to infinity, depending on the definition of the restoring force $r(x)$ for larger x in the model). See e.g. Belenky (1993) for a closed form solution to the capsizing probability of the model (1.1) with a piecewise linear restoring force.

A numerical method to compute (estimate) capsizing probabilities for the model (1.1) and also for more realistic and analytically intractable systems (such as the actual dynamics of a ship) was proposed by Belenky et al. (2008) and coined *split-time*. See also Belenky et al. (2016, 2023) for an up-to-date review of the method. In the split-time approach, calculation of the capsizing probability is reduced to two separate less complex problems: one, the so-called *non-rare* problem, involves the rate of the upcrossing of an intermediate level of a roll motion and, second, the so-called *rare* problem that focuses on capsizing after an upcrossing. In the latter (rare) problem, a roll rate

* Correspondence to: Department of Statistics and Operations Research, UNC at Chapel Hill, CB#3260, Hanes Hall, Chapel Hill, NC 27599, USA.
E-mail addresses: diglotzer@meredith.edu (D. Glotzer), pipiras@email.unc.edu (V. Pipiras), vadim.belenky@navy.mil (V. Belenky), kenneth.weems@navy.mil (K.M. Weems), sapsis@mit.edu (T.P. Sapsis).

https://doi.org/10.1016/j.oceaneng.2023.116538
Received 25 May 2023; Received in revised form 1 December 2023; Accepted 10 December 2023
Available online 23 December 2023

leading to capsizing is computed numerically at each upcrossing, called a *critical response rate*. A split-time metric of capsizing is then formed as the difference between the observed and the critical response rates, with a positive difference corresponding to capsizing. The probability of capsizing after upcrossing can then be found by extrapolating the tail of the distribution of the split-time metric using the generalized Pareto distribution (GPD) as suggested by Extreme Value Theory (see e.g. Coles (2001)). The form of the GPD is recalled in Section 2.2. The key advantage of the split-time method is that it lends itself to reproducing a rare phenomenon such as capsizing, which would be too costly to simulate directly with a simulation tool of reasonable fidelity. The split-time method was applied to another rare event, the so-called broaching-to in Belenky et al. (2017).

Though we are not aware of the split-time technique employed for other rare phenomena, the approach is reminiscent of ideas employed in the global stability analysis of dynamical systems. This is related, in particular, to the domains (regions, basins) of attraction – the sets of initial conditions with trajectories leading to a particular attractor (equilibrium point) – especially in the context of multi-stable dynamical systems (Battelino et al., 1988). Recent numerical methods for computing these domains and related quantities include (Najafi et al., 2016; Datseris and Wagemakers, 2022; Stender and Hoffmann, 2022).

One striking feature of the GPD use is that it commonly suggests the distribution of the critical response rate (and the split-time metric) having "light" tails, characterized by a negative or zero shape parameter of the GPD (e.g., Belenky et al. (2023)). In contrast, the distribution of the response itself often has a "heavy" right tail, especially in rough seas, characterized by a positive shape parameter of the GPD. The latter phenomenon and, more generally, the tail structure of the distribution of the response itself in the model (1.1) was studied and clarified by Belenky et al. (2019), in the case of both correlated and white noise excitations. In particular, a heavier distribution tail was the result of softening restoring nonlinearity. In this work, we attempt to provide an analysis similar to Belenky et al. (2019) but for the distributions of the critical response rate (rather than the response itself) and split-time metric. More specifically, our goals are to: (i) Confirm the light character of the distribution tail of the critical response rate and split-time metric for some forms of the nonlinear oscillator (1.1), for both correlated and white noise excitations, (ii) Provide insight into the structure of the distribution tail of the critical response rate and split-time metric, and (iii) Understand implications of the findings on extreme value analysis of the considered distributions. To the best of our knowledge, this is the first paper to take a closer look at the distribution of the critical response rate in a nonlinear oscillator (1.1) and its distribution tails.

Regarding the third point above, our theoretical and empirical analysis suggests that the distribution of the split-time metric is in the domain of maxima attraction of the GPD with zero shape parameter, that is, the exponential distribution. This motivates the use of the exponential distribution, rather than the GPD, for exceedances above threshold in extreme value analysis. We investigate this approach for the derived distributions of the split-time metric, by using threshold selection based on goodness-of-fit tests for the exponential distribution. In fact, the exponential distribution was used for peaks over threshold in Hydrology before the GPD was adopted as a more flexible model, though threshold selection was made based on other considerations (e.g. Rosbjerg et al. (1992) and Todorovic and Zelenhasic (1970)).

Finally, we compare the approach of peaks over threshold with the exponential distribution to that with the distribution having a Weibull tail. While the exponent in the exponential distribution has a power equal to one, the power of the exponent in a Weibull-tailed distribution can be different from one. For example, the tail of a Gaussian distribution is Weibull-tailed with the exponent equal to two. All Weibull-tailed distributions are in the domain of maxima attraction of the exponential distribution, but they offer a more refined representation of distribution tails. In fact, our theoretical analysis of the distribution of the split-time metric point to a Weibull tail and thus suggests using the approach of peaks over threshold with Weibull-tailed distributions.

The paper by Belenky et al. (2023) also examines questions around the split-time metric, but the focus there is on data and numerics from ship motion programs and the context of ship stability. In contrast, this study concerns the oscillator model and the data generated from this model, providing complementary perspectives to the work of Belenky et al. (2019). We also note that some elements of this work appeared previously in the conference papers by Belenky et al. (2018a,b).

The rest of the paper is organized as follows. Section 2 includes some preliminary background, specifying the exact cases of the model (1.1) considered in this work, and also recalling the GPD and its use in Extreme Value Theory and in working with the split-time metric. The considered models are piecewise linear and doubly piecewise linear oscillators with a correlated excitation, and a softening Duffing oscillator with a white noise excitation. The distribution and its tails for the critical response rate (and the split-time metric) in these models are studied in Section 3. Section 4 contains some numerical results on the distributions of the critical response rate and the split-time metric. Section 5 concerns the use of the exponential distribution and the distribution with a Weibull tail for peaks over threshold. Conclusions can be found in Section 6.

2. Preliminaries

2.1. Description of models

We are interested in a single-degree-of-freedom nonlinear oscillator given by (1.1), where $\delta > 0$ is the damping parameter, $y(t)$ is a random, mean zero excitation process and $r(x)$ is the restoring force. More specifically, two forms of stochastic excitation are considered: correlated and white noise. The correlated excitation is assumed to be a mean zero, stationary Gaussian process with the spectral density motivated by the ship rolling application, namely,

$$s_y(\omega) = \omega_0^4 \left(\frac{\omega^2}{g}\right)^2 s_w(\omega), \quad \omega > 0, \tag{2.1}$$

where ω is wave frequency, ω_0 is a natural frequency (both frequencies in rad/s), and $g = 9.807$ rad/s is gravitational acceleration. The Bretschneider spectral density $s_w(\omega)$ is taken for wave elevation:

$$s_w(\omega) = \frac{A}{\omega^5} e^{-\frac{B}{\omega^4}}, \quad \omega > 0, \tag{2.2}$$

where $A = 173 H_s^2 T_1^{-4}$ and $B = 691 T_1^{-4}$ both depend on significant wave height, H_s (in meters), and the period corresponding to mean frequency of waves, T_1 (in seconds). The factor ω^2/g in (2.1) is a wave number or spatial frequency of linear waves, and accounts for the roll motion being excited through the wave slope or wave spatial derivative. The factor ω_0^4 accounts for the roll motion being excited by a moment of hydrodynamic pressure forces.

The white noise excitation, on the other hand, can be viewed as a (generalized) derivative of the Wiener process, that is, $y(t) = \sigma_f \dot{W}(t)$, and as having a constant spectral density

$$s_y(\omega) = \sigma_f^2, \tag{2.3}$$

where $\sigma_f > 0$ determines the strength of the excitation. Though the broadband nature of the white noise forcing is certainly not realistic for describing wave excitation, its use in the ship rolling application is still relevant, since the ship roll motion is dominated by ship motion inertia. Working with the white noise excitation will allow for more analytic calculations with the model (1.1) that cannot be carried out assuming correlated excitation.

In the case of correlated excitations, two types of the nonlinear restoring force are considered. The *piecewise linear* restoring force is

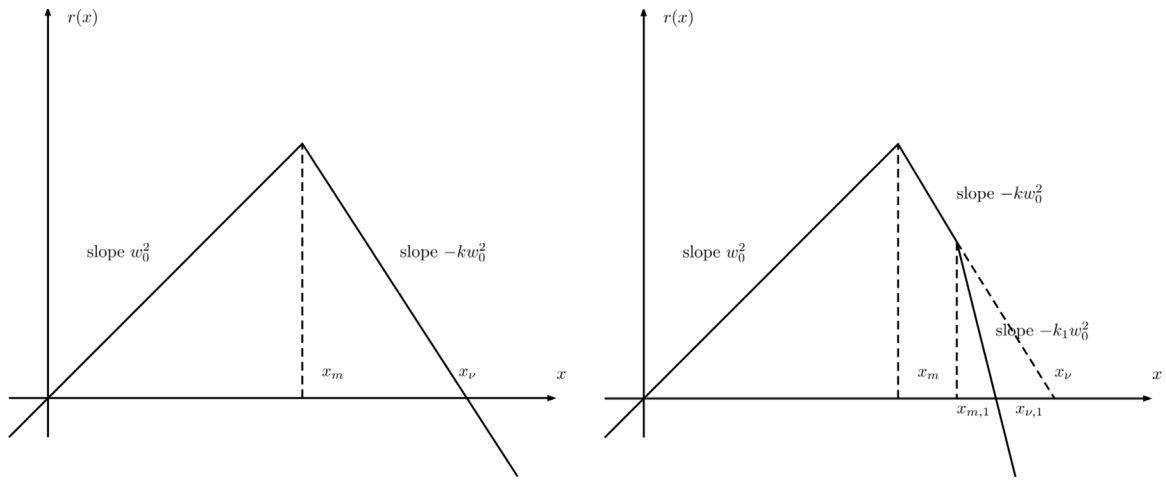

Fig. 1. The PWL (left plot) and DPWL (right plot) restoring forces.

given by

$$r(x) = \begin{cases} -kw_0^2\left(x + x_m\right) - w_0^2 x_m, & \text{if } x < -x_m, \\ w_0^2 x, & \text{if } -x_m \le x \le x_m, \\ -kw_0^2\left(x - x_m\right) + w_0^2 x_m, & \text{if } x > x_m, \end{cases} \tag{2.4}$$

where w_0 is a natural frequency in the linear regime $(-x_m, x_m)$, $-kw_0^2 < 0$ is a negative slope in the nonlinear regime $|x| > x_m$ with $k > 0$ and x_m, called the "knuckle" point, defines the threshold above which the system behaves nonlinearly, i.e. the point above which the restoring force is decreasing. We shall refer to the oscillator associated with the restoring force (2.4) as *piecewise linear* (*PWL*).

The *doubly piecewise linear* restoring force is given by: for $x > 0$ and with $k_1 > 0$,

$$r(x) = \begin{cases} w_0^2 x, & \text{if } 0 < x \le x_m, \\ -kw_0^2\left(x - x_m\right) + w_0^2 x_m, & \text{if } x_m < x \le x_{m,1}, \\ -k_1 w_0^2\left(x - x_{m,1}\right) - kw_0^2\left(x_{m,1} - x_m\right) + w_0^2 x_m, & \text{if } x_{m,1} < x, \end{cases} \tag{2.5}$$

and $r(-x) = r(x)$. It thus makes the decreasing linear part of the piecewise linear restoring force to be piecewise linear itself. We shall refer to the oscillator associated with the restoring force (2.5) as *doubly piecewise linear* (*DPWL*).

We denote the respective points of vanishing stability, that is, the points for which the restoring force becomes zero, by x_ν for the PWL oscillator, and by $x_{\nu,1}$ for the DPWL oscillator. The restoring forces and the introduced notation for the PWL and DPWL oscillators are depicted in Fig. 1.

Though the use of a piecewise linear restoring force may seem unnatural in connection to realistic forces, this turns out to be a useful idealization that allows for analytic arguments in the case of correlated excitation, and also retains most known nonlinear properties of an oscillator with a similar smooth stiffness (Belenky, 2000; Belenky et al., 2019). We consider the DPWL oscillator to assess how our findings for the PWL system are affected by further nonlinearity in the restoring force.

In the case of the white noise excitation (2.3), we shall consider the restoring force

$$r(x) = kx - cx^3, \quad k > 0, c > 0, \tag{2.6}$$

associated with a softening Duffing oscillator. The methods described in this paper are general enough to accommodate other nonlinear restoring forces, although the calculations may be less tractable.

2.2. Split-time metric and its extrapolation through GPD

In the context of ship motions, the split-time metric gives a way to describe how close one came to capsizing, even when capsizing did not occur, conditioned on having crossed an intermediate threshold (that is commonly taken to be large). The split-time metric is defined as

$$d_{\text{st}} = 1 + \dot{x}_1 - \dot{x}_{\text{cr}}, \tag{2.7}$$

where $\dot{x}_1$ is the observed response rate at the moment of upcrossing of the threshold, and $\dot{x}_{\text{cr}}$ is the critical response rate which would lead to capsizing. The value of the metric gives a "distance" to capsizing. In particular, $d_{\text{st}} \ge 1$ corresponds to capsizing, and $d_{\text{st}} < 1$ corresponds to not capsizing. The probability of capsizing is then expressed as

$$\begin{aligned} \mathbb{P}(\text{capsizing}) &= \mathbb{P}(\text{crossing threshold}) \cdot \mathbb{P}(d_{\text{st}} \ge 1 | \text{crossing threshold}) \\ &=: \mathbb{P}(\text{crossing threshold}) \cdot \mathbb{P}^*(d_{\text{st}} \ge 1), \end{aligned} \tag{2.8}$$

where $\mathbb{P}^*$ refers to the conditional probability.

To estimate $\mathbb{P}$(capsizing), a system of interest (e.g. (1.1)) is simulated until a chosen intermediate threshold is crossed, at which point the simulation is paused and the critical rate is found through a step search, after which the procedure is continued till multiple values of d_{st} are collected and multiple crossings have occurred. The probability $\mathbb{P}$(crossing threshold) can be estimated directly from the crossing frequency. On the other hand, the probability $\mathbb{P}^*(d_{\text{st}} \ge 1)$ is estimated by applying techniques from Extreme Value Theory, as no observed values of d_{st} would typically be bigger than 1. More specifically, the peaks-over-threshold (POT) approach (see e.g. Glotzer et al. (2017) or Coles (2001)) is used, by writing first:

$$\mathbb{P}^*(d_{\text{st}} \ge 1) = \mathbb{P}^*(d_{\text{st}} > u)\mathbb{P}^*(d_{\text{st}} \ge 1 | d_{\text{st}} > u), \tag{2.9}$$

where u is an intermediate threshold of d_{st} smaller than 1 and for which there are $d_{\text{st}} > u$. The non-rare probability $\mathbb{P}^*(d_{\text{st}} > u)$ is estimated as the observed proportion of d_{st}'s exceeding u. The rare probability $\mathbb{P}^*(d_{\text{st}} \ge 1 | d_{\text{st}} > u)$ is estimated by fitting a generalized Pareto distribution to d_{st} above u and using it to extrapolate to the capsizing value $d_{\text{st}} = 1$.

It is well known that under general conditions the distribution of exceedances above a sufficiently large threshold from a sequence of i.i.d. (independent identically distributed) random variables is well approximated by a generalized Pareto distribution (GPD; see e.g. Pickands (1975) or Coles (2001)). Its complementary distribution function is

$$\overline{F}_{\mu,\xi,\sigma}(x) = \begin{cases} \left(1 + \frac{\xi(x-\mu)}{\sigma}\right)^{-1/\xi}, & \mu < x, \quad \text{if } \xi > 0, \\ e^{-\frac{x-\mu}{\sigma}}, & \mu < x, \quad \text{if } \xi = 0, \\ \left(1 + \frac{\xi(x-\mu)}{\sigma}\right)^{-1/\xi}, & \mu < x < \mu - \frac{\sigma}{\xi}, \quad \text{if } \xi < 0, \end{cases} \tag{2.10}$$

where the parameters are ξ (shape), and σ (scale), and μ (threshold, equal to u in (2.9)). The sign of the shape parameter determines whether the tail of the GPD is light ($\xi \leq 0$) or heavy ($\xi > 0$). A GPD with a light tail has an upper bound at $\mu+(-\sigma/\xi)$ when $\xi < 0$, while a heavy tail has a power-law form. When $\xi = 0$, the GPD is the exponential distribution.

We also note that in theory, distributions having a power-law tail are approximated by (are in the domain of attraction of) the GPD with positive shape parameter $\xi > 0$. Likewise, the domain of attraction of GPD with negative shape parameter $\xi < 0$ are distributions having an upper finite bound and a suitable power-law behavior at that bound. In fact, most other "light" distributions (normal, Weibull, etc.) are in the domain of attraction of an exponential distribution, that is, the GPD with $\xi = 0$. In practice, the situation is a bit complex. For example, estimated shape parameters for a normal distribution would typically be negative, since the normal tail is lighter than the exponential tail. From this more practical perspective, the GPD can be thought as a flexible family of models for distribution tails, whose nature can range from power laws (i.e. very heavy) to bounded from above (i.e. very light). Though we also emphasize that this view is too simplistic, since the GPD arises naturally in Extreme Value Theory as the distribution to use for exceedances above large thresholds.

3. Distributions of response rates

We study here the distributions of the critical response rate and the split-time metric for the models listed in Section 2.1: the PWL and DPWL oscillators with correlated excitation (Sections 3.1 and 3.2 below) and the Duffing oscillator with white noise excitation (Section 3.3 below).

3.1. PWL oscillator with correlated excitation

We are interested here in a critical response rate, that is, the rate needed to capsize at the upcrossing of the process $x(t)$ of the level x_m. We denote the value of the critical response rate as $\dot{x}_{cr}$. The crossing level is naturally taken as the "knuckle" point x_m since the system transitions into a nonlinear regime above this point.

For the PWL oscillator, the solution after the upcrossing of the process of the level x_m is given by

$$x(t) = Ae^{\lambda_1 t} + Be^{\lambda_2 t} + x_v, \tag{3.1}$$

when the excitation is switched off after the upcrossing, and

$$x(t) = Ae^{\lambda_1 t} + Be^{\lambda_2 t} + x_v + p_u(t), \tag{3.2}$$

when the excitation is present. Switching off excitation above the "knuckle" point is natural since most of the excitation is expected to be received through resonance which is not possible when the stiffness is decreasing (see e.g. Belenky and Sevastianov (2007)). Here, A and B are constants determined by the initial conditions $x(0) = x_m$ and $\dot{x}(0) = \dot{x}_1$,

$$\lambda_1 = -\delta + \sqrt{kw_0^2 + \delta^2} > 0, \quad \lambda_2 = -\delta - \sqrt{kw_0^2 + \delta^2} < 0, \tag{3.3}$$

and $p_u(t)$ is a particular solution after the upcrossing, that is, the process satisfying

$$\ddot{p}_u(t) + 2\delta\dot{p}_u(t) - kw_0^2 p_u(t) = y(t) \tag{3.4}$$

and such that at time 0, the process $x(t)$ satisfying the linear equation

$$\ddot{x}(t) + 2\delta\dot{x}(t) + w_0^2 x(t) = y(t) \tag{3.5}$$

upcrosses x_m. For later reference, we also let $p(t)$ be the process satisfying

$$\ddot{p}(t) + 2\delta\dot{p}(t) - kw_0^2 p(t) = y(t), \tag{3.6}$$

without conditioning on the upcrossing of $x(t)$.

With the excitation switched off, we have

$$A = \frac{\dot{x}_1 + \lambda_2(x_v - x_m)}{\lambda_1 - \lambda_2}, \quad B = -\frac{\lambda_1(x_v - x_m) + \dot{x}_1}{\lambda_1 - \lambda_2} \tag{3.7}$$

and with the excitation on,

$$A = \frac{\dot{x}_1 - \dot{p}_1 + \lambda_2(x_v + p_1 - x_m)}{\lambda_1 - \lambda_2}, \quad B = -\frac{\lambda_1(x_v + p_1 - x_m) + \dot{x}_1 - \dot{p}_1}{\lambda_1 - \lambda_2}, \tag{3.8}$$

where $p_1 = p_u(0)$ and $\dot{p}_1 = \dot{p}_u(0)$. The system capsizes when $A > 0$, leading to the following critical response rates: with the excitation switched off,

$$\dot{x}_{\text{cr}} = -\lambda_2(x_v - x_m) \tag{3.9}$$

and with the excitation on,

$$\dot{x}_{\text{cr}} = -\lambda_2(x_v - x_m + p_1) + \dot{p}_1. \tag{3.10}$$

Note that $\dot{x}_{\text{cr}}$ is constant when the excitation is switched off. To understand the distribution of $\dot{x}_{\text{cr}}$ when the excitation is switched on, we need to characterize the joint distribution of p_1 and $\dot{p}_1$. We shall make a simplifying assumption that before the upcrossing of x_m, the process $x(t)$ behaves as a Gaussian process, satisfying Eq. (3.5). This simplifying assumption is often made in the literature (e.g. Mohamad and Sapsis (2015)), and has been studied closer in Belenky et al. (2019).

By using a standard argument (e.g. Lindgren (2013), Section 8.3; Sólnes (1997), 161-162), the density of $\dot{x}_1$, p_1 and $\dot{p}_1$ at the upcrossing of x_m is given by

$$C_0 \dot{x} f_{\mu_0,\Sigma_0}(x_m, \dot{x}, p, \dot{p}), \tag{3.11}$$

where C_0 is a normalizing constant, $f_{\mu,\Sigma}$ denotes the multivariate normal density with mean μ and variance Σ, and

$$\mu_0 = \begin{pmatrix} 0 \\ 0 \\ 0 \\ 0 \end{pmatrix}, \quad \Sigma_0 = \begin{pmatrix} \sigma_x^2 & \sigma_{x\dot{x}} & \sigma_{xp} & \sigma_{x\dot{p}} \\ \sigma_{\dot{x}x} & \sigma_{\dot{x}}^2 & \sigma_{\dot{x}p} & \sigma_{\dot{x}\dot{p}} \\ \sigma_{px} & \sigma_{p\dot{x}} & \sigma_p^2 & \sigma_{p\dot{p}} \\ \sigma_{\dot{p}x} & \sigma_{\dot{p}\dot{x}} & \sigma_{\dot{p}p} & \sigma_{\dot{p}}^2 \end{pmatrix} \tag{3.12}$$

with the entries in Σ_0 denoting the corresponding covariances of the processes satisfying (3.4) and (3.5). In particular, $\sigma_{x\dot{x}} = 0$, $\sigma_{p\dot{p}} = 0$ and $\sigma_{x\dot{p}} = -\sigma_{\dot{x}p}$.

The normal density in (3.11) can be simplified and expressed more conveniently through several conditioning arguments as follows. Note that

$$f_{\mu_0,\Sigma_0}(x_m, \dot{x}, p, \dot{p}) = f(x_m) f(\dot{x}, p, \dot{p} | x = x_m), \tag{3.13}$$

where f's on the right-hand side of the equation refer to the density of x and the conditional density of $\dot{x}, p, \dot{p}$ given $x = x_m$. As x_m is constant, so is $f(x_m)$ and it can be incorporated into the normalizing constant in (3.11). On the other hand, a conditional distribution of a multivariate normal distribution is known to be normal as well and for the case of interest here, it can be computed as follows. Let $\Sigma_{0,\dot{x}p\dot{p}}$ denote the 3×3 submatrix of Σ_0 associated with the variables $\dot{x}$, p and $\dot{p}$, $\Sigma_{0,\dot{x}p\dot{p}|x}$ denote the 3×1 vector $(\sigma_{x\dot{x}}\ \sigma_{xp}\ \sigma_{x\dot{p}})$ consisting of covariances for $\dot{x}$, p, $\dot{p}$ and x, respectively, $\Sigma_{0,x} = \sigma_x^2$ and $\mu_{0,\dot{x}p\dot{p}}$ denote the 3×1 zero vector of the means associated with $\dot{x}$, p and $\dot{p}$, and $\mu_{0,x} = 0$. The conditional density in (3.13) is then the normal density $f_{\mu_1,\Sigma_1}(\dot{x}, p, \dot{p})$ with the mean and covariance given by

$$\mu_1 = \mu_{0,\dot{x}p\dot{p}} + \Sigma_{0,\dot{x}p\dot{p}|x}\Sigma_{0,x}^{-1}(x_m - \mu_{0,x}) = \begin{pmatrix} 0 \\ \frac{\sigma_{px}}{\sigma_x^2} x_m \\ \frac{\sigma_{\dot{p}x}}{\sigma_{\dot{x}}^2} x_m \end{pmatrix} =: \begin{pmatrix} 0 \\ \bar{p} \\ \bar{\dot{p}} \end{pmatrix}, \tag{3.14}$$

$$\Sigma_1 = \Sigma_{0,\dot{x}p\dot{p}} - \Sigma_{0,\dot{x}p\dot{p}|x}\Sigma_{0,x}^{-1}\Sigma'_{0,\dot{x}p\dot{p}|x} = \begin{pmatrix} \sigma_{\dot{x}}^2 & \sigma_{\dot{x}p} & \sigma_{\dot{x}\dot{p}} \\ \sigma_{p\dot{x}} & \sigma_p^2 - \frac{\sigma_{px}^2}{\sigma_x^2} & -\frac{\sigma_{px}\sigma_{\dot{p}x}}{\sigma_x^2} \\ \sigma_{\dot{p}\dot{x}} & -\frac{\sigma_{px}\sigma_{\dot{p}x}}{\sigma_x^2} & \sigma_{\dot{p}}^2 - \frac{\sigma_{\dot{p}x}^2}{\sigma_x^2} \end{pmatrix} \tag{3.15}$$

(see e.g. Timm (2002), Section 3.3a). By this conditioning procedure, we can thus rewrite the density (3.11) as

$$C_1 \dot{x} f_{\mu_1,\Sigma_1}(\dot{x}, p, \dot{p}), \tag{3.16}$$

where x_m is now absorbed into C_1 and μ_1.

By using another conditioning but now on the variable $\dot{x}$ and the notation analogous to above, we can express the density (3.16) as

$$\frac{\dot{x}}{\sigma_{\dot{x}}^2} e^{-\dot{x}^2/(2\sigma_{\dot{x}}^2)} f_{\mu_2(\dot{x}),\Sigma_2}(p, \dot{p}), \tag{3.17}$$

where

$$\mu_2(\dot{x}) = \mu_{1,p\dot{p}} + \Sigma_{1,p\dot{p}|\dot{x}} \Sigma_{1,\dot{x}}^{-1} (\dot{x} - \mu_{1,\dot{x}}) = \begin{pmatrix} \bar{p} + \frac{\sigma_{p\dot{x}}}{\sigma_{\dot{x}}^2}\dot{x} \\ \bar{\dot{p}} + \frac{\sigma_{\dot{p}\dot{x}}}{\sigma_{\dot{x}}^2}\dot{x} \end{pmatrix} = \begin{pmatrix} \frac{\sigma_{px}}{\sigma_x^2} x_m + \frac{\sigma_{p\dot{x}}}{\sigma_{\dot{x}}^2}\dot{x} \\ \frac{\sigma_{\dot{p}x}}{\sigma_x^2} x_m + \frac{\sigma_{\dot{p}\dot{x}}}{\sigma_{\dot{x}}^2}\dot{x} \end{pmatrix}, \tag{3.18}$$

$$\Sigma_2 = \Sigma_{1,p\dot{p}} - \Sigma_{1,p\dot{p}|\dot{x}} \Sigma_{1,\dot{x}}^{-1} \Sigma_{1,p\dot{p}|\dot{x}}' = \begin{pmatrix} \sigma_p^2 - \frac{\sigma_{px}^2}{\sigma_x^2} - \frac{\sigma_{p\dot{x}}^2}{\sigma_{\dot{x}}^2} & -\frac{\sigma_{px}\sigma_{\dot{p}x}}{\sigma_x^2} - \frac{\sigma_{p\dot{x}}\sigma_{\dot{p}\dot{x}}}{\sigma_{\dot{x}}^2} \\ -\frac{\sigma_{px}\sigma_{\dot{p}x}}{\sigma_x^2} - \frac{\sigma_{\dot{p}x}\sigma_{\dot{p}\dot{x}}}{\sigma_{\dot{x}}^2} & \sigma_{\dot{p}}^2 - \frac{\sigma_{\dot{p}x}^2}{\sigma_x^2} - \frac{\sigma_{\dot{p}\dot{x}}^2}{\sigma_{\dot{x}}^2} \end{pmatrix}. \tag{3.19}$$

The expression (3.17) for the density of $\dot{x}_1$, p_1 and $\dot{p}_1$ shows that, as expected, $\dot{x}_1$ follows the Rayleigh distribution with parameter $\sigma_{\dot{x}}^2$, and that conditionally on $\dot{x}_1$, the distribution of p_1 and $\dot{p}_1$ is bivariate normal with mean vector $\mu_2(\dot{x}_1)$ and covariance matrix Σ_2. Note that only the mean depends on $\dot{x}_1$.

These findings suggest that in practice, a sample of independent copies of the vector $(p_1, \dot{p}_1)'$ can be generated easily, and then substituted into (3.10) to get a sample of independent copies of $\dot{x}_{\mathrm{cr}}$, whose distribution can then be examined using available exploratory tools. This is pursued further in Section 4.

We note that an explicit expression for the density of p_1 and $\dot{p}_1$ can also be obtained, after integrating out the variable $\dot{x}$ in (3.17). But its form is quite lengthy and will not be presented here. The same could also be said about the distribution of the critical response rate. In fact, as illustrated in Section 4 below, the distribution of the latter is close to a normal distribution. This perhaps should not be that surprising since the distribution of p_1 and $\dot{p}_1$ is (conditionally) normal. In particular, the distribution tails of $\dot{x}_{\mathrm{cr}}$ are determined by the normal distribution tails of p_1 and $\dot{p}_1$.

The arguments presented above extend naturally to the split-time metric defined in (2.7), that is,

$$d_{\mathrm{st}} = 1 + \dot{x}_1 - \dot{x}_{\mathrm{cr}} = \begin{cases} 1 + \dot{x}_1 + \lambda_2(x_v - x_m), & \text{with excitation off,} \\ 1 + \dot{x}_1 + \lambda_2 \\ \quad \times (x_v - x_m + p_1) - \dot{p}_1, & \text{with excitation on,} \end{cases} \tag{3.20}$$

in view of (3.9) and (3.10). Thus, with excitation off, the distribution of the metric is just a shifted Rayleigh distribution. That is, the distribution of the metric and its tail are completely determined by those of the response rate at the upcrossing. When excitation is on, a sample of independent copies of the metric d_{st} can be generated efficiently in the same way as for $\dot{x}_{\mathrm{cr}}$ discussed above and examined through available exploratory tools. The latter is pursued further in Section 4 below.

In fact, the asymptotic behavior of the distribution tail of d_{st} with turned on excitation can be derived easily. It follows from (3.17)–(3.19) that the density of d_{st} is

$$f_{d_{\mathrm{st}}}(y) = \int_0^\infty d\dot{x} \int_{\mathbb{R}} dp \, \frac{\dot{x}}{\sigma_{\dot{x}}^2} e^{-\dot{x}^2/(2\sigma_{\dot{x}}^2)} f_{\mu_2(\dot{x}),\Sigma_2}(p, \dot{x} + \lambda_2 p - y), \quad y \in \mathbb{R}. \tag{3.21}$$

Indeed, both integrals can be evaluated analytically. First, we rewrite the multivariate normal density as a univariate normal density in p (only) by completing the square, i.e. writing

$$f_{\mu_2(\dot{x}),\Sigma_2}(p, \dot{x} + \lambda_2 p - y) \propto e^{-\frac{1}{2}(Ap^2 - 2Bp + C)} = e^{-\frac{A}{2}(p - \frac{B}{A})^2} \, e^{-\frac{1}{2}\left(C - \frac{B^2}{A}\right)},$$

where $\propto$ denotes "proportional to", and B and C depend on $\dot{x}$ and y, while A is a constant with respect to both. This allows writing the density as

$$\begin{aligned} f_{d_{\mathrm{st}}}(y) &\propto \int_0^\infty d\dot{x} \, \dot{x} e^{-\frac{\dot{x}^2}{2\sigma_{\dot{x}}^2}} e^{-\frac{1}{2}\left(C - \frac{B^2}{A}\right)} \int_{\mathbb{R}} f_{\frac{B}{A},\frac{1}{A}}(p) dp \\ &= \int_0^\infty d\dot{x} \, \dot{x} e^{-\frac{\dot{x}^2}{2\sigma_{\dot{x}}^2} - \frac{1}{2}\left(C - \frac{B^2}{A}\right)}, \quad y \in \mathbb{R}, \end{aligned} \tag{3.22}$$

where f_{μ,σ^2} denotes the univariate normal density as in the multivariate case. It can be seen that the exponent of the exponential function is quadratic in both $\dot{x}$ and y. A second application of completing the square allows rewriting the exponential term with $\dot{x}$ only, i.e.

$$f_{d_{\mathrm{st}}}(y) \propto e^{-\frac{1}{2}\left(C_0 - \frac{B_0^2}{A_0}\right)} \int_0^\infty d\dot{x} \, \dot{x} e^{-\frac{A_0}{2}\left(\dot{x} + \frac{B_0}{A_0}\right)^2}, \quad y \in \mathbb{R}, \tag{3.23}$$

where A_0 is a constant, B_0 is linear in y, and C_0 is quadratic in y.

Next, we evaluate the remaining integral by a simple change of variables. In particular,

$$\int_0^\infty d\dot{x} \, \dot{x} e^{-\frac{1}{2}A_0\left(\dot{x} + \frac{B_0}{A_0}\right)^2} = \frac{1}{A_0}\left[e^{-\frac{B_0^2}{2A_0}} + B_0\sqrt{\frac{\pi}{2A_0}}\left(\mathrm{erf}\left(\frac{B_0}{\sqrt{2A_0}}\right) - 1\right)\right],$$

where $\mathrm{erf}(x) = \frac{2}{\sqrt{\pi}} \int_0^x e^{-u^2} du$. Hence,

$$\begin{aligned} f_{d_{\mathrm{st}}}(y) &\propto e^{-\frac{1}{2}\left(C_0 - \frac{B_0^2}{A_0}\right)}\left[e^{-\frac{B_0^2}{2A_0}} + B_0\sqrt{\frac{\pi}{2A_0}}\left(\mathrm{erf}\left(\frac{B_0}{\sqrt{2A_0}}\right) - 1\right)\right] \\ &= e^{-\frac{C_0}{2}} + \sqrt{\frac{\pi}{2A_0}} B_0 e^{-\frac{1}{2}\left(C_0 - \frac{B_0^2}{A_0}\right)}\left(\mathrm{erf}\left(\frac{B_0}{2\sqrt{A_0}}\right) - 1\right), \quad y \in \mathbb{R}. \end{aligned}$$

Letting $B_0' := \frac{B_0}{\sqrt{2A}}$, we can rewrite this as

$$f_{d_{\mathrm{st}}}(y) \propto e^{-\frac{C_0}{2}}\left[1 + \sqrt{\pi} B_0' e^{B_0'^2}\left(\mathrm{erf}\left(B_0'\right) - 1\right)\right], \quad y \in \mathbb{R}. \tag{3.24}$$

Now, $1 + \sqrt{\pi} x e^{x^2}(\mathrm{erf}(x) - 1) \sim (2x^2)^{-1}$, as $x \to \infty$. Since C_0 is quadratic in y and B_0 is linear in y, it follows from (3.24) that, as $y \to \infty$,

$$f_{d_{\mathrm{st}}}(y) \sim a \frac{e^{-b(y-c)^2}}{y^2},$$

for some constants a, b, c. Then, the tail of the corresponding CDF satisfies: as $x \to \infty$,

$$\begin{aligned} \int_x^\infty f_{d_{\mathrm{st}}}(y) dy &\sim a \int_x^\infty \frac{e^{-b(y-c)^2}}{y^2} dy \sim ab^{1/2} \int_{b^{1/2}(x-c)}^\infty \frac{e^{-z^2}}{z^2} dz \\ &\sim ab^{1/2} \frac{e^{-(b^{1/2}(x-c))^2}}{2(b^{1/2}(x-c))^3} \sim \frac{ae^{-b(x-c)^2}}{2bx^3}, \end{aligned} \tag{3.25}$$

where the asymptotic relation before last can be derived by integration by parts and the asymptotics of the tail of normal CDF (e.g. Small (2010), p. 44). Thus, one can write the tail of the CDF as

$$\int_x^\infty f_{d_{\mathrm{st}}}(y) dy = e^{-L(x)x^2}, \tag{3.26}$$

where the function $L(x)$ is such that $L(x) \to b$ as $x \to \infty$. The CDF tail then has the form (5.3) in Section 5.2 below and as noted in that section, it is in the domain of attraction of the GPD with shape parameter $\xi = 0$.

Finally, we note that since $\dot{x} > 0$, the second argument $\dot{x} + \lambda_2 p - y$ of the bivariate normal density can only get larger as $y \to -\infty$ and hence the integrand of (3.21) can only get smaller. On the other hand, $y \to \infty$ could be compensated by larger $\dot{x} > 0$ in the same second argument. This suggests that the left-tail of the density (3.21) is lighter than the right tail. We also see this in the numerical illustrations in Section 4.1.

3.2. DPWL oscillator with correlated excitation

We now turn to the DPWL oscillator, and suppose that the excitation is present in the regime $x_m < x < x_{m,1}$ but is switched off in the regime $x > x_{m,1}$. As in (3.9), we know that the critical response rate in the regime $x > x_{m,1}$ is

$$\dot{x}_{\mathrm{cr},1} = -\lambda_{2,1}(x_{v,1} - x_{m,1}), \tag{3.27}$$

where as in (3.3),

$$\lambda_{1,1} = -\delta + \sqrt{k_1 w_0^2 + \delta^2} > 0, \quad \lambda_{2,1} = -\delta - \sqrt{k_1 w_0^2 + \delta^2} < 0. \tag{3.28}$$

Since the solution in the regime $x_m < x < x_{m,1}$ is still given by (3.2), the critical response rate for the DPWL oscillator should now satisfy: with $\dot{x} = \dot{x}_{\mathrm{cr}}$ and $t = t_{\mathrm{cr}}$,

$$\begin{cases} A(\dot{x})e^{\lambda_1 t} + B(\dot{x})e^{\lambda_2 t} + x_v + p_u(t) = x_{m,1}, \\ \lambda_1 A(\dot{x})e^{\lambda_1 t} + \lambda_2 B(\dot{x})e^{\lambda_2 t} + pu'(t) = -\lambda_{2,1}(x_{v,1} - x_{m,1}), \end{cases} \tag{3.29}$$

where $A = A(\dot{x})$ and $B = B(\dot{x})$ are given in (3.8).

We are interested in solving (3.29) numerically. In order to do so, we need to understand the structure of the process $p_u(t)$. By arguing as for the PWL system in Section 3.2, one can show that conditionally on $\dot{x} = \dot{x}_1$, the process $p_u(t)$ is Gaussian with mean

$$\mu_{p_u}(t) = \frac{\gamma_{xp}(t)}{\sigma_x^2} x_m + \frac{\gamma_{\dot{x}p}(t)}{\sigma_{\dot{x}}^2} \dot{x} \tag{3.30}$$

and covariance function

$$\gamma_{p_u}(t_1, t_2) = \gamma_p(t_1 - t_2) - \frac{\gamma_{xp}(t_1)\gamma_{xp}(t_2)}{\sigma_x^2} - \frac{\gamma_{\dot{x}p}(t_1)\gamma_{\dot{x}p}(t_2)}{\sigma_{\dot{x}}^2}, \tag{3.31}$$

where

$$\gamma_p(t) = \mathbb{E}p(0)p(t), \quad \gamma_{xp}(t) = \mathbb{E}x(0)p(t), \quad \gamma_{\dot{x}p}(t) = \mathbb{E}\dot{x}(0)p(t)$$

and $x(t)$ satisfies the linear Eq. (3.5), and $p(t)$ satisfies the linear Eq. (3.6). Thus, one can write

$$p_u(t) = \frac{\gamma_{xp}(t)}{\sigma_x^2} x_m + \frac{\gamma_{\dot{x}p}(t)}{\sigma_{\dot{x}}^2} \dot{x} + \kappa(t), \tag{3.32}$$

where $\kappa(t)$ is a Gaussian zero mean process with the same covariance as $p_u(t)$, that is,

$$\mathbb{E}\kappa(t_1)\kappa(t_2) = \gamma_p(t_1 - t_2) - \frac{\gamma_{xp}(t_1)\gamma_{xp}(t_2)}{\sigma_x^2} - \frac{\gamma_{\dot{x}p}(t_1)\gamma_{\dot{x}p}(t_2)}{\sigma_{\dot{x}}^2}, \tag{3.33}$$

This representation is known as the Slepian model for the particular solution $p(t)$ after the upcrossing of $x(t)$ of the level x_m. See e.g. Lindgren (2013), Section 8.4. The next elementary lemma clarifies the structure of the process $\kappa(t)$.

Lemma 3.1. *With the above notation, we have the following representation:*

$$\kappa(t) = p(t) - \frac{\gamma_{xp}(t)}{\sigma_x^2} x(0) - \frac{\gamma_{\dot{x}p}(t)}{\sigma_{\dot{x}}^2} \dot{x}(0). \tag{3.34}$$

Proof. The proof is elementary by checking that the process on the right-hand side of (3.34) has the covariance function (3.31). □

By using (3.34), the representation (3.32) of the particular solution $p_u(t)$ can also be expressed as

$$p_u(t) = \frac{\gamma_{xp}(t)}{\sigma_x^2}(x_m - x(0)) + \frac{\gamma_{\dot{x}p}(t)}{\sigma_{\dot{x}}^2}(\dot{x} - \dot{x}(0)) + p(t). \tag{3.35}$$

This representation of $p_u(t)$ is most convenient when generating $p_u(t)$ in practice.

Several approximations of $p_u(t)$ can be tried when substituting (3.35) into (3.29). One approximation is

$$p_{u,\mathrm{app},1}(t) = \frac{\gamma_{xp}(0) + \gamma'_{xp}(0)t}{\sigma_x^2}(x_m - x(0)) + \frac{\gamma_{\dot{x}p}(0) + \gamma'_{\dot{x}p}(0)t}{\sigma_{\dot{x}}^2}(\dot{x} - \dot{x}(0))$$

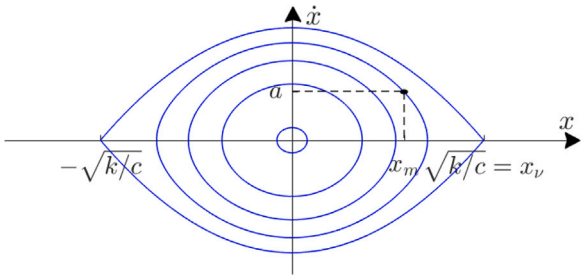

Fig. 2. A phase portrait of the Duffing oscillator, restricted to the heteroclinical orbit connecting the unstable equilibria $\pm\sqrt{k/c}$.

$$\begin{aligned} &+p(0) + p'(0)t \\ &= \frac{\sigma_{xp} + \sigma_{x\dot{p}}t}{\sigma_x^2}(x_m - x(0)) + \frac{\sigma_{\dot{x}p} + \sigma_{\dot{x}\dot{p}}t}{\sigma_{\dot{x}}^2}(\dot{x} - \dot{x}(0)) \\ &+p(0) + p'(0)t. \end{aligned} \tag{3.36}$$

This approximation linearizes the covariance functions in (3.35) as $\gamma_{xp}(t) \simeq \gamma_{xp}(0) + \gamma'_{xp}(0)t$ and $\gamma_{\dot{x}p}(t) \simeq \gamma_{\dot{x}p}(0) + \gamma'_{\dot{x}p}(0)t$, and the process $p(t)$ in (3.35) as $p(t) \simeq p(0) + p'(0)t$. As illustrated in Section 4, this approximation is accurate till about $t = 1$. Another approximation is

$$p_{u,\mathrm{app},2}(t) = \frac{\gamma_{xp}(t)}{\sigma_x^2}(x_m - x(0)) + \frac{\gamma_{\dot{x}p}(t)}{\sigma_{\dot{x}}^2}(\dot{x} - \dot{x}(0)) + p(0) \tag{3.37}$$

(or without $p(0)$), which only simplifies the process $p(t)$ in (3.35) to $p(0)$. This approximation does not appear accurate for larger t – keep in mind that the process $p(t)$ is stationary and its magnitude does not seem negligible. See Section 4.

In Section 4, we will report on the distributions of the critical response rate $\dot{x}_{\mathrm{cr}}$ when solving (3.29) numerically, and also the distribution of the resulting split-time metric. The findings are similar to those for the PWL oscillator.

3.3. Duffing oscillator with white noise excitation

We now turn to the Duffing oscillator with the restoring force $r(x)$ in (2.6) and the white noise excitation $y(t) = \sigma_f \dot{W}(t)$ characterized by (2.3). Fig. 2 depicts a qualitative phase portrait of the (undamped, unforced) system, limited to the heteroclinical orbit connecting the two unstable equilibria $x_v = \pm\sqrt{k/c}$. The point of upcrossing $x(0) = x_m$ and the upcrossing response rate $\dot{x}(0) = a$ are also marked in the plot.

We define capsizing as crossing the heteroclinical orbit connecting the two unstable equilibrium without later coming back to it and again are interested in a critical response rate $\dot{x}_{\mathrm{cr}}$. Note that the rate $\dot{x}_{\mathrm{cr}}$ depends only on a future realization of white noise (and the upcrossing threshold x_m). Capsizing, on the other hand, will also depend on the rate at the upcrossing. In our calculations, we shall make the simplifying assumption that capsizing is "monotone" in the rate, that is, if a given rate leads to capsizing, then so would any larger rate (for a given future realization of white noise).

Since the critical response rate is defined as the rate leading to capsizing, note that

$$\mathbb{P}_{x_m}(\dot{x}_{\mathrm{cr}} \le a) = \mathbb{P}_{x_m}(\mathrm{capsize}|\dot{x}(0) = a), \tag{3.38}$$

where $\mathbb{P}_{x_m}$ denotes a probability with respect to a future realization of white noise, conditioned on $x(0) = x_m$. The white noise realizations in the two events of (3.38) are the same: if a white noise realization is such that $\dot{x}_{\mathrm{cr}} \le a$, then by monotonicity, one should be capsizing with any larger velocity, including $\dot{x}(0) = a$; vice versa, if one is capsizing for a white noise realization with $\dot{x}(0) = a$, then by monotonicity, this also means that $\dot{x}_{\mathrm{cr}} \le a$ for such a realization.

In the rest of this section, we focus on computing the CDF of the critical response rate $\dot{x}_{\text{cr}}$ using the right-hand side of (3.38). Strictly speaking, our calculations will be approximate and expected to be accurate only in certain regions. More specifically, to evaluate the capsizing probability of interest, we consider only short time intervals, which allows one to remove damping for its insignificant role and to assume a small variance of the excitation. A short time interval can be assumed if one is close to the heteroclinical orbit or if an initial displacement $x(0) = x_m$ is large. Two cases must be handled separately, according to whether the initial conditions a, x_m are within or beyond the heteroclinical orbit.

We first consider the case of starting within the orbit. Under the assumptions above, we shall find the mean and the variance of the maximum response which will lead to the probability of interest by conditioning on the maximum response being above the unstable equilibrium $x_v = \sqrt{k/c}$. Fig. 3, left plot, illustrates our approach.

Under the assumptions above, the equation for the mean $\overline{x}(t)$ of the process is

$$\ddot{\overline{x}}(t) + k\overline{x}(t) - c\overline{x}(t)^3 = 0; \quad \dot{\overline{x}}(0) = a, \quad \overline{x}(0) = x_m. \tag{3.39}$$

By conservation of energy, the mean $\overline{x}_{\max}$ of the maximum response conditional on $\dot{\overline{x}}(t) = 0$ satisfies

$$k\overline{x}_{\max}^2 - \frac{1}{2}c\overline{x}_{\max}^4 = a^2 + kx_m^2 - \frac{1}{2}cx_m^4 =: 2E(a, x_m). \tag{3.40}$$

Solving this equation gives

$$\overline{x}_{\max} = \sqrt{\frac{-k + \sqrt{k^2 - 2(a^2 + kx_m^2 - \frac{1}{2}cx_m^4)c}}{-c}}, \tag{3.41}$$

which depends in a direct way on the initial conditions a, x_m. On the heteroclinical orbit, $E(a, x_m) = \frac{k^2}{2c}$, so (3.41) simplifies to $\overline{x}_{\max} = x_v$.

Similarly, we can calculate the variance. The period of the nonlinear oscillator can be computed as follows. Note that, over a quarter of a period $T_0(a, x_m)$, we should have $x(t)$ go from 0 to $\overline{x}_{\max}$. Then,

$$\frac{T_0(a, x_m)}{4} = \int_0^{\overline{x}_{\max}} \frac{dx}{\sqrt{2E(a, x_m) - kx^2 + \frac{1}{2}cx^4}}. \tag{3.42}$$

For each choice of a, x_m, to make calculations tractable, substitute the nonlinear oscillator with a linear one having the same natural period of oscillation:

$$\ddot{x}^*(t) + \omega_0^2(a, x_m)x^*(t) = \sigma_f \dot{W}(t), \quad \omega_0(a, x_m) = \frac{2\pi}{T_0(a, x_m)}, \tag{3.43}$$

where $x^*(t)$ is the fluctuation around the mean $\overline{x}(t)$ which is due to white noise. For this system, we have

$$\sigma_{x^*}^2(t) := \mathbb{E}x^*(t)^2 = \frac{\sigma_f t}{\omega_0^2(a, x_m)} - \frac{\sigma_f(\sin 2\omega_0(a, x_m)t)}{2\omega_0^3(a, x_m)} \tag{3.44}$$

(see e.g. Gitterman (2005), Section 8.2, p. 85). The time it takes for the system to go from $(x(0), \dot{x}(0)) = (a, x_m)$ to $(\overline{x}_{\max}, 0)$ is

$$T_{\max}(a, x_m) = \int_{x_m}^{\overline{x}_{\max}} \frac{dx}{\sqrt{2E(a, x_m) - kx^2 + \frac{1}{2}cx^4}}. \tag{3.45}$$

This time has to be relatively small for our analysis to be valid. Thus,

$$\sigma_{x^*}^2\Big|_{\overline{x}_{\max}} = \frac{\sigma_f T_{\max}(a, x_m)}{\omega_0^2(a, x_m)} - \frac{\sigma_f(\sin 2\omega_0(a, x_m)T_{\max}(a, x_m))}{2\omega_0^3(a, x_m)}. \tag{3.46}$$

In view of the developments above, we conclude that, under the heteroclinical orbit,

$$\mathbb{P}_{x_m}(\text{capsize}|\dot{x}(0) = a) = \int_{x_v}^{\infty} \varphi(u; \overline{x}_{\max}, \sigma_{x^*}^2\Big|_{\overline{x}_{\max}})du, \tag{3.47}$$

where $\varphi(u; \mu, \sigma^2)$ is the density of a normal distribution with mean μ and variance σ^2. Note that both $\overline{x}_{\max}$ and $\sigma_{x^*}^2\Big|_{\overline{x}_{\max}}$ depend on a and x_m.

After a change of variables, and by (3.38), we can write the CDF of the critical rate (under the heteroclinical orbit) as

$$F_{\dot{x}_{\text{cr}}}(a) = \overline{\Phi}((x_v - \overline{x}_{\max})/\sigma_{x^*}\Big|_{\overline{x}_{\max}}), \tag{3.48}$$

where $\overline{\Phi}(z) = \mathbb{P}(N(0, 1) > z)$ is the tail of the CDF of the standard normal distribution.

We now turn to the case of initial conditions being above the heteroclinical orbit. This approach is illustrated in Fig. 3, right plot. Here, capsizing occurs for trajectories which remain outside the heteroclinical orbit. Since $\overline{x}(t)$ has no maximum in this case, we consider its variability when $\dot{x}(t)$ is minimized. It is straightforward to see from (3.40) that

$$\dot{x}(t) = \sqrt{2E(a, x_m) - kx(t)^2 + \frac{1}{2}cx(t)^4}, \tag{3.49}$$

which is minimized when $x(t) = x_v$, hence

$$\dot{x}_{\min} = \sqrt{2E(a, x_m) - \frac{1}{2}\frac{k^2}{c}}. \tag{3.50}$$

We assume that the time it takes for $x(t)$ to go from 0 to x_v is a quarter of a period, i.e. (3.42) and (3.45) still apply, with $\overline{x}_{\max}$ replaced by $\dot{x}_{\min}$. Thus, the variability, characterized by $\sigma_{x^*}^2\Big|_{\dot{x}_{\min}}$, is computed as in (3.46). The probability of capsizing additionally depends on the (horizontal) distance from $(x(t), \dot{x}(t)) = (x_v, \dot{x}_{\min})$ to $(x_{\text{het}}, \dot{x}_{\min})$, where $x_{\text{het}} = x_{\text{het}}(a, x_m)$ is on the heteroclinical orbit. From (3.49), we find

$$x_{\text{het}} = \sqrt{\frac{k - \sqrt{2c\dot{x}_{\min}^2 - k^2}}{c}}, \tag{3.51}$$

and

$$F_{\dot{x}_{\text{cr}}}(a) = \overline{\Phi}((x_{\text{het}} - x_v)/\sigma_{x^*}\Big|_{\overline{x}_{\max}}). \tag{3.52}$$

Calculations involved in differentiating to compute the density of the critical rate have proven unwieldy. Simulation for the distributions (3.48) and (3.52) are discussed in Section 4 below.

An argument can be extended to generate observations of $\dot{x}$, $\dot{x}_{\text{cr}}$ and hence those of the split-time metric. Since $\dot{x}_1$ depends on a past realization of white noise and $\dot{x}_{\text{cr}}$ depends on the future, the joint density of the rate and critical rate is given by

$$f_{x_m}(\dot{x}_1 = b, \dot{x}_{\text{cr}} = a) = f_{x_m}(\dot{x}_1 = b)f_{x_m}(\dot{x}_{\text{cr}} = a), \tag{3.53}$$

where the density of $\dot{x}(0)$ is known explicitly from the Fokker–Planck-Kolmogorov equation, yielding

$$f_{x_m}(\dot{x}(0) = a) = Ce^{-\frac{2\delta}{\sigma_f^2}a^2}, \tag{3.54}$$

where C is a normalizing constant. See e.g. Belenky et al. (2019), Eq. (3.1), and Sobczyk (1991), Theorem 1.6, p. 34 or p. 334. It follows that the density of the split-time metric d_{st} is

$$f_{x_m}(d_{\text{st}} = z) = f_{x_m}(\dot{x}_1 - \dot{x}_{\text{cr}} = z - 1) = \int_0^{\infty} f_{x_m}(\dot{x}_1 = u + z - 1)f_{x_m}(\dot{x}_{\text{cr}} = u)du.$$

By Eqs. (3.48) and (3.3), and using integration by parts, we can write

$$\begin{aligned} f_{x_m}(d_{\text{st}} = z) &= \int_0^{\infty} Ce^{-\frac{2\delta}{\sigma_f^2}(u+z-1)^2} dF_{\dot{x}_{\text{cr}}}(u) \\ &= C_2 \int_0^{\infty} F_{\dot{x}_{\text{cr}}}(u)(u + z - 1)e^{-\frac{2\delta}{\sigma_f^2}(u+z-1)^2} du, \end{aligned} \tag{3.55}$$

where C_2 is a normalizing constant.

4. Numerical results

We shall examine here the distributions of the critical response rate and the split-time metric for the PWL and DPWL systems and the Duffing oscillator through some available exploratory tools. This includes simulation from these systems, both their direct simulation and from the derived distribution of interest, and visual exploratory analysis.

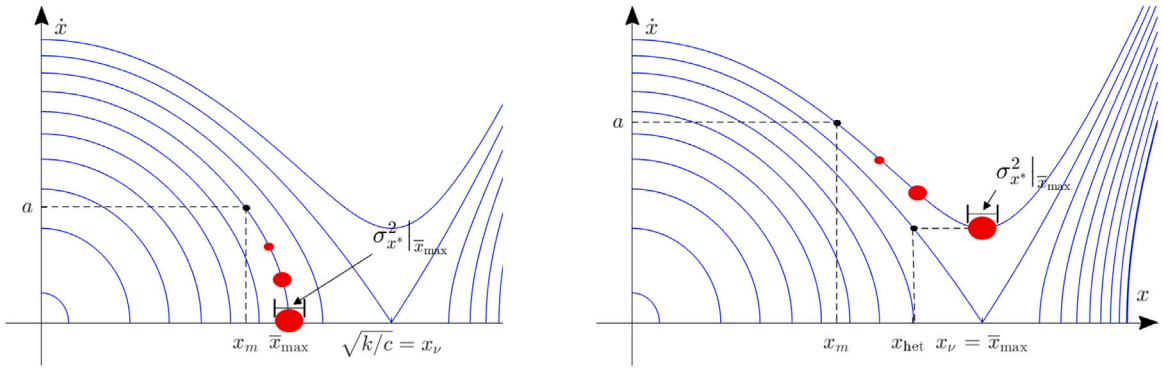

Fig. 3. The path of $\overline{x}(t)$ to $\overline{x}_{\max}(a, x_m)$ and its variability characterized by $\sigma^2_{x^*}\big|_{\overline{x}_{\max}}$, for choices of a within (left) and beyond (right) the heteroclinical orbit connecting the two unstable equilibria.

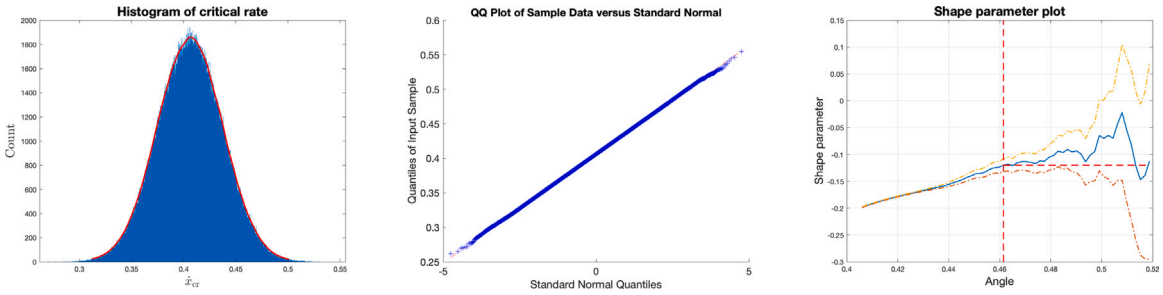

Fig. 4. The critical response rate for the PWL oscillator: Left: histogram with a numerically computed density; Middle: QQ-plot; Right: the shape parameter plot for the right tail.

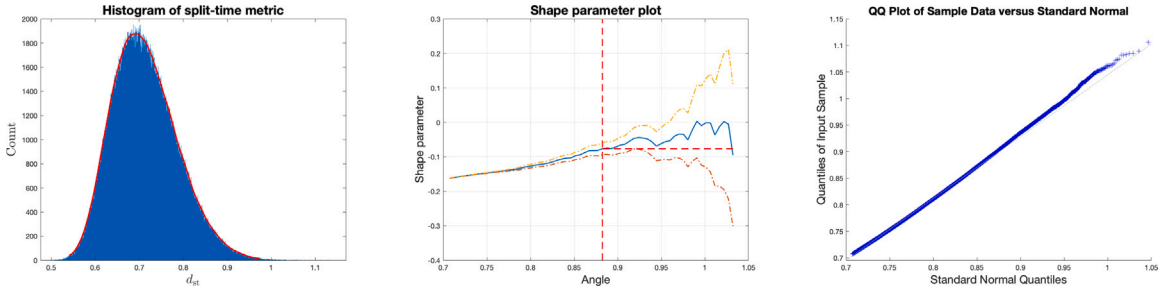

Fig. 5. The split-time metric from the PWL oscillator: Left: histogram with a numerically computed density; Middle: the shape parameter plot for the right tail; Right: the QQ-plot of the metric above median with the right-tail of a standard normal distribution.

Table 1
Parameter values in simulations.

Parameter	PWL simulation	DPWL simulation
w_0	0.6	0.6
δ	$0.15w_0 = 0.09$	0.09
x_m	$30\pi/180 = 0.52$	0.52
$x_{m,1}$	–	$x_m + \frac{1}{2}(x_\nu - x_m)$
k	0.5	0.5
k_1	–	1.5
H_s	9	9
T_m	15	15

4.1. PWL and DPWL oscillators

We generated 500,000 independent observations of the critical response rates for the PWL oscillator, and 5,000 for the DPWL oscillator. The parameter values for either set of the simulations are given in Table 1, and are identical with the exception of the decreasing linear segments of the restoring forces. See Fig. 1 for the graphical representation of the forces.

Fig. 4 depicts several exploratory plots for the critical response rate generated from the PWL oscillator. The left plot shows the histogram and numerically computed density. The middle plot is the standard normal quantile plot. The right plot is the shape parameter plot for the right distribution tail, that is, the plot of estimated shape parameter values with confidence intervals against selected thresholds. The confidence bands are indicated in dashed dotted lines, in yellow for the upper boundary and in red for the lower boundary. A horizontal dashed line starts from the smallest threshold for which the estimate falls within confidence bands for all larger thresholds. The histogram and numerically computed density appear normal. The quantile plot shows little deviation from normal quantiles, except perhaps with slightly lighter tails. The shape parameter plot for the right tail estimate a shape parameter of about $\xi = -0.1$, although $\xi = 0$ is not outside the confidence bounds, which is consistent with the estimated shape parameter from the normal distribution. Thus, all three plots suggest agreement that the distribution of the critical response rate is close to normal. As the quantile plot shows alignment with the normal distribution in both tails and the normal distribution tails are symmetric, the shape parameter plot for the left tail is unsurprisingly similar to that for the right tail and is excluded for shortness sake. The shape parameter plot

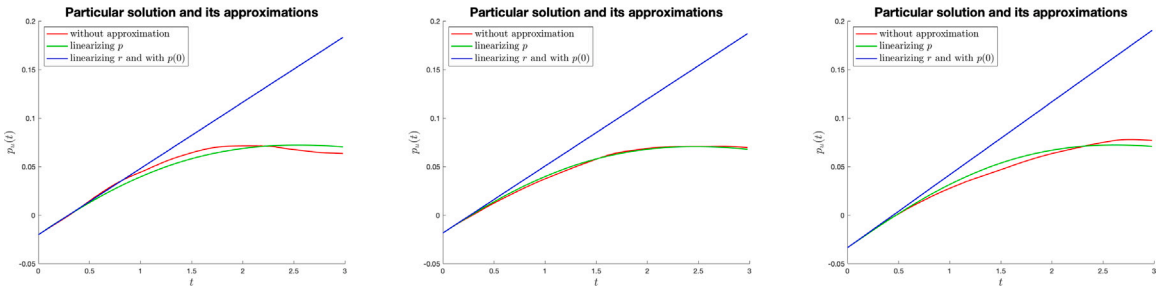

Fig. 6. The particular solution (after the upcrossing of the process) and its approximations. The three plots are for three realizations.

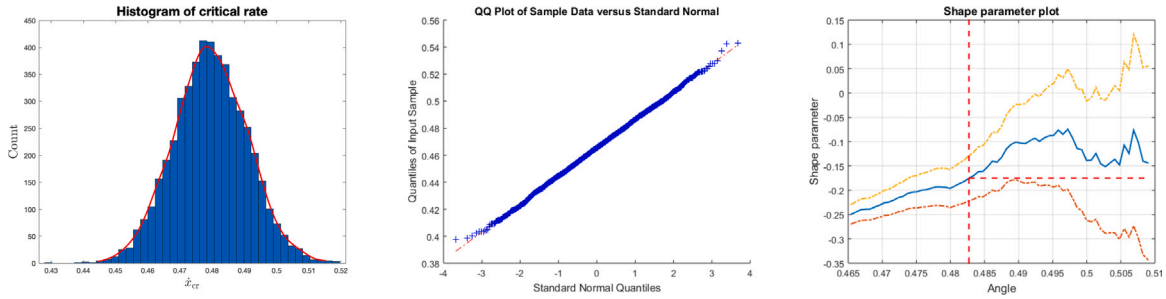

Fig. 7. The critical response rate from the DPWL oscillator: Left: histogram; Middle: QQ-plot; Right: the shape parameter plot for the right tail.

for the right tail is included, in part, to illustrate how such plots look for distributions with normal-like tails. Fig. 5 shows similar plots but for the split-time metric from the PWL oscillator, focusing on the behavior of the right tail. The plots similarly suggest that the tail appears close to that of a normal distribution.

Considering the DPWL oscillator, three realizations of the particular solutions $p_u(t)$ and its two approximations discussed in Section 3.2 are depicted in Fig. 6 solely for illustration purposes. The plots suggest that the first approximation (linearizing p, in green) is quite accurate, typically until approximately $t = 1$, and that the second approximation (linearizing r, in blue) is less accurate.

By using the parameter values above, we generated 5,000 independent copies of the critical response rates for the DPWL oscillator. Fig. 7 depicts the histogram, the normal quantile plot, and the shape parameter plot for the right tail, as in Fig. 4. The results of the exploratory analysis are not too different from those for the PWL oscillator. In particular, the distribution of the critical response rate is close to normal: the histogram appears normal, and the quantile plot may indicate a lighter tail on the left, and a heavier tail on the right, as compared to the normal distribution. The shape parameter plot estimates a shape parameter of about $\xi = -0.2$, and $\xi = 0$ is not outside the confidence bounds, which is consistent with the estimated shape parameter from a normal distribution. Thus, all three plots suggest that the distribution of the critical response rate is close to normal. The figure of the split-time metric for the DPWL oscillator also turns out to be similar to Fig. 5 for the PWL oscillator and is excluded for shortness sake.

4.2. Duffing oscillator

Here, we compare the oscillators above to the Duffing oscillator discussed in Section 3.3. We generated 10,000 independent copies of the critical response rate with parameter values $\omega_0, \delta, H_s, T_m$, as in Table 1, and $x_m = 0.3$, $k = 1$, $c = 3$. For the excitation, $\sigma_f = 0.0730$, to approximately match the frequency of upcrossings of x_m as would occur in the linear case.

The CDF of the critical rate (see (3.38), (3.47), (3.48) and (3.52)) was numerically calculated for values of a from 0 to 3 with a stepsize of 0.0005, and the density was estimated through differencing. The sample is gathered from this density through rejection sampling and its histogram and estimated density are depicted in Fig. 8 (left plot). The middle and right plots show the shape parameter plots for both the right and left tails; unsurprisingly, negative shape parameters are estimated in both cases. The shape parameter plot for the left tail is given as that for the right tail of the critical rate values taken with a negative sign.

Additional 10,000 independent copies of the split-time metric were generated directly from independent samples of the rate (taken from a half-normal distribution) and critical rate, and following Eq. (2.7). Exploratory plots are depicted in Fig. 9, including a histogram with a numerically computed density, a shape parameter plot for the right tail, and a QQ-plot for the right tail only. As in the cases of the PWL and DPWL oscillators discussed in Section 4.1, a shape parameter value of $\xi = 0$ is within confidence bounds, which is consistent the tail of a normal distribution. The QQ-plot though indicates some deviation from a normal tail.

5. Implications for extreme value analysis and other distribution fits

We discuss here briefly several statistical implications of the findings in the previous sections, namely, concerning the uses of the exponential distribution (Section 5.1) and the distribution with a Weibull tail (Section 5.2) in the POT approach.

5.1. POT approach with exponential distribution

The results of Sections 3 and 4 suggest (and in some cases show) that the distribution of the split-time metric for the considered models is in the domain of maxima attraction of the GPD with the shape parameter $\xi = 0$, that is, the exponential distribution. A natural question then is whether the POT approach described in Section 2.2 could be used with the exponential distribution for extrapolation above threshold, instead of the GPD. In fact, the POT approach has originated in Hydrology with using the exponential distribution for POT (see e.g. Ekanayake and Cruise (1993), Madsen et al. (1993) and references therein) though the setting in these early works is slightly different from that considered here (e.g. a threshold is selected based on the

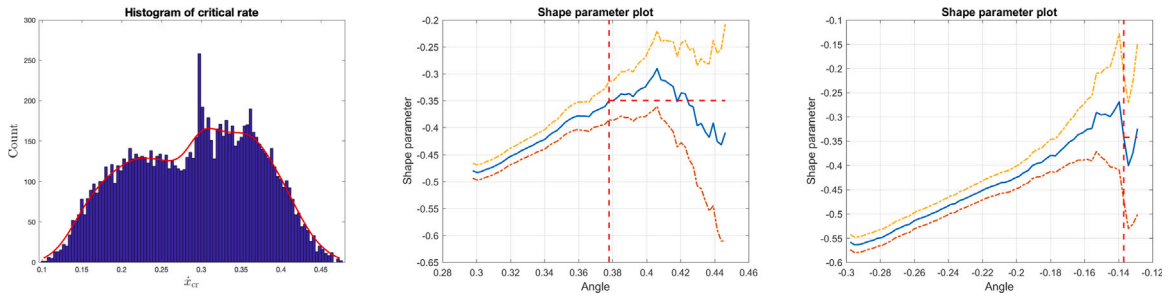

Fig. 8. The critical response rate from the Duffing oscillator: Left: histogram with a numerically estimated density; Middle: the shape parameter plot for the right tail; Right: the shape parameter plot for the left tail.

Fig. 9. The split-time metric from the Duffing oscillator: Left: histogram with a numerically estimated density; Middle: the shape parameter plot for the right tail; Right: the QQ-plot of the metric with the right-tail of a standard normal distribution.

exceedance times following a Poisson process). We also note that fitting the exponential distribution above threshold is essentially equivalent to fitting the Gumbel distribution (one of the three extreme value distributions) to block maxima (e.g. see Gomes and Guillou (2015)).

In attempting to use the POT approach with the exponential distribution, the choice of a threshold (denoted u in (2.9)) is critical. The methods of threshold selection that we have been using are based on either the goodness-of-fit tests for the exponential distributions (Spineili and Stephens, 1987) or a prediction error criterion (Mager, 2015). In the first approach, for a range of intermediate thresholds, we would test if the data above a given threshold is consistent with the exponential distribution (at some significance level α) and then choose the smallest threshold for which this consistency holds (the null hypothesis not rejected), including all larger thresholds. But we also found that for this method to work, the significance level should be quite large (say $\alpha = 30\%$ or 40%). Choosing large α will lead to larger selected threshold and fewer observations above the threshold, and thus also larger associated uncertainty (wider confidence intervals).

In the second approach, a threshold is chosen based on a prediction error criterion. More specifically, let $X_{n,n} \le \cdots \le X_{1,n}$ be the order statistics of a variable of interest, for example, the split-time metric d_{st}. A threshold $u = X_{k+1,n}$ or the index k is then selected as

$$\hat{k} = \arg\min_{k} \hat{\Gamma}(k). \tag{5.1}$$

Here, the minimum is searched over some range of values k, with Mager (2015) suggesting to use $k \in [\max(40, 0.02n), 0.2n]$, though in simulations for synthetic distributions, we sometimes find the results to be sensitive to the choice of upper bound. The quantity $\hat{\Gamma}(k)$ is defined as

$$\begin{aligned}\hat{\Gamma}(k) = \hat{\sigma}^{-2} \sum_{i=1}^{k} \left(\frac{k+1}{i} - 1\right)^{-1} \left(X_{i,n} - u + \hat{\sigma} \log\left(\frac{i}{k+1}\right)\right)^2 \\ + \frac{2}{k} \sum_{i=1}^{k} \left(\frac{k+1}{i} - 1\right)^{-1} \log^2\left(\frac{i}{k+1}\right) - 1,\end{aligned} \tag{5.2}$$

where $\hat{\sigma}$ is the scale parameter estimate of the exponential distribution based on $X_{i,n} - u$, $i = 1, \ldots, k$. See Mager (2015), bottom of p. 64.

Fig. 10 illustrates the POT approaches based on the GPD (left plot) and the exponential distribution (middle plot), applied to extrapolating the distribution of the absolute value of the standard normal random variable with sample size $n = 1000$. A threshold for both methods is selected automatically by using the prediction error criterion mentioned above and found in Mager (2015). Each vertical line corresponds to a separate independent replication, with the circle indicating the estimate of the exceedance probability $\mathbb{P}(|N(0,1)| > 4.056) = 5{\times}10^{-5}$ and the line corresponding to the associated 95% confidence interval, all on a log vertical scale. The horizontal line shows the target probability 5×10^{-5}. As expected, about 95% of the vertical lines include the true probability in both GPD and exponential cases. But note that that confidence intervals for the exponential case are narrower, which might be an appealing feature for using the POT approach with the exponential distribution in practice — again this is assuming the knowledge that the data is from the distribution in the domain of attraction of the exponential distribution, as suggested e.g. for the split-time metric through the models analyzed above.

5.2. POT approach for distribution with Weibull tail

Instead of using the POT approach with the exponential distribution, another interesting alternative is to use a POT approach for a distribution having a Weibull tail. More specifically, supposing X is a variable of interest (say positive), it is said to have a Weibull tail if

$$\mathbb{P}(X > x) = e^{-L(x)x^{1/\theta}}, \quad x > 0, \tag{5.3}$$

where θ is a parameter and $L(x)$ is a slowly varying function at infinity, satisfying $L(ax)/L(x) \to 1$ as $x \to \infty$ for any fixed $a > 0$. Distributions with Weibull tails are of interest here for several reasons. First, the split-time metric in the models considered in Section 3 was either proved or strongly suggested to have a Weibull tail (with $\theta = 0.5$); see (3.26). Second, from the GPD perspective, a distribution with a Weibull tail falls in the domain of attraction of the GPD with zero shape parameter, that is, the exponential distribution (e.g. Proposition 2, (ii) in Gardes et al. (2011)). Distributions with Weibull tails then provide an interesting flexible family of distribution tails for extrapolation when in

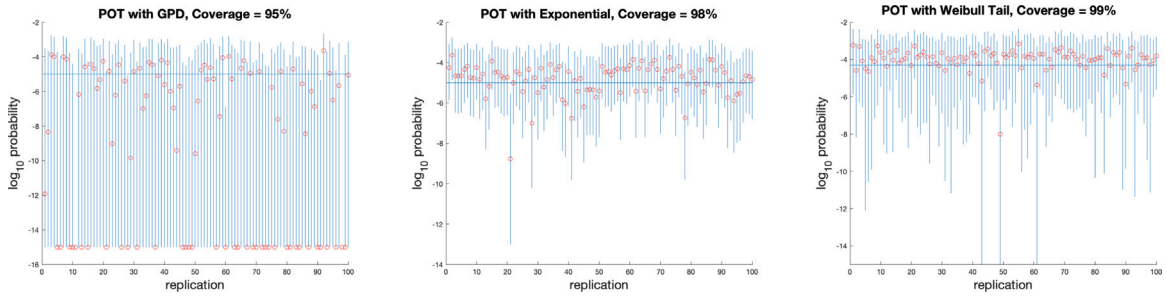

Fig. 10. The POT approaches based on the GPD (left plot), the exponential (middle plot) and the Weibull-tailed (right plot) distributions.

such a domain of attraction. Third, the parameter θ and its existence are informative on their own. Fourth, as noted below, there is an analogous POT approach for distributions with Weibull tails.

Indeed, numerous works in Extreme Value Analysis concern estimation of θ and related questions. See, for example, Gardes and Girard (2005, 2006), Diebolt et al. (2008), Asimit et al. (2010) and Gardes et al. (2011). The POT approach for a distribution with a Weibull tail is based on the observation that, for some critical value of interest $x_{\rm cr}$,

$$\begin{aligned}\log \mathbb{P}(X > x_{\rm cr}) &= \log \mathbb{P}(X > u)\frac{\log \mathbb{P}(X > x_{\rm cr})}{\log \mathbb{P}(X > u)} \\ &= \log \mathbb{P}(X > u)\frac{L(x_{\rm cr})x_{\rm cr}^{1/\theta}}{L(u)u^{1/\theta}} \approx (\log \mathbb{P}(X > u))\left(\frac{x_{\rm cr}}{u}\right)^{1/\theta},\end{aligned} \tag{5.4}$$

where u is an intermediate threshold and we used (5.3). As with the usual POT approach involving GPD, the non-rare probability is estimated directly from the data as a suitable sample proportion. The rest of the procedure involves estimation of θ with a confidence interval and also setting a threshold u.

The issue of threshold selection is seemingly not quite resolved in the literature. See, in particular, Asimit et al. (2010), Statement 1, and also Mercadier and Soulier (2012), Section 4. The approach that we use adapts an ad hoc approach of Reiss and Thomas for GPD (see Neves and Fraga Alves (2004)), wherein the usual bias–variance tradeoff in estimation is exploited. More specifically, an index k in $u = X_{k+1,n}$ (as in Section 5.1, $X_{i,n}, i = 1, \dots, n$ denotes the order statistic) is chosen as

$$\widehat{k} = \arg\min_k \frac{1}{k}\sum_{i=1}^{k} i^{\beta}\left|\widehat{\theta}_k - \text{median}\left(\widehat{\theta}_1, \dots, \widehat{\theta}_k\right)\right|, \tag{5.5}$$

where $\beta \in (0, \frac{1}{2}]$ is fixed and $\widehat{\theta}_k$ is an estimate of θ based on $X_{i,n}, i = 1, \dots, k$. Moreover, the minimum is often considered for $k \geq K$ for some fixed K (e.g. $K = 20$). Fig. 10, right plot, presents analogous estimation results based on the POT approach with Weibull tail. The results are comparable to the POT approach based on the exponential distribution, though the latter tends to have slightly smaller confidence intervals.

6. Conclusions

In this work, we examined the distributions of the critical response rate and split-time metric of the nonlinear oscillator given in (1.1). We considered several forms of the restoring force, including piecewise linear and doubly piecewise linear stiffness functions, as well as a cubic restoring from the Duffing oscillator; and both correlated and white noise excitations. The distributions were examined analytically in some cases and also numerically, using techniques from Extreme Value Theory such as the POT approach. Due to the nature of the observed tail of the distributions of both the critical response rate and the split-time metric, we considered modifying the POT approach to fit either an exponential distribution or a Weibull tail for peaks above threshold.

CRediT authorship contribution statement

Dylan Glotzer: Formal analysis, Methodology, Software, Writing – original draft. **Vladas Pipiras:** Conceptualization, Formal analysis, Methodology, Software, Writing – original draft. **Vadim Belenky:** Conceptualization, Methodology, Writing – review & editing. **Kenneth M. Weems:** Conceptualization, Methodology, Writing – review & editing. **Themistoklis P. Sapsis:** Conceptualization, Formal analysis, Methodology, Writing – original draft.

Declaration of competing interest

The authors declare that they have no known competing financial interests or personal relationships that could have appeared to influence the work reported in this paper.

Data availability

Data will be made available on request.

Acknowledgments

The authors are grateful to two anonymous Reviewers for their many useful comments and suggestions. The work described in this paper has been funded by the Office of Naval Research (ONR), United States under Dr. Thomas Fu and Dr. Woei-Min Lin and by the Naval Surface Warfare Center Carderock Division (NSWCCD) Independent Applied Research (IAR) program. Participation of Prof. Pipiras was facilitated by the Summer Faculty Program supported by ONR and managed by NSWCCD under Dr. Jack Price, who also manages IAR program. Participation of Mr. Glozter was facilitated by the NSWCCD Naval Research Enterprise Internship Program (NREIP) program managed by Ms. Rachel Luu. Prof. Pipiras also acknowledges the partial support of the ONR, United States grants N00014-19-1-2092 and N00014-23-1–2176 at the University of North Carolina.

References

Asimit, A.V., Li, D., Peng, L., 2010. Pitfalls in using Weibull tailed distributions. J. Statist. Plann. Inference 140 (7), 2018–2024.

Battelino, P.M., Grebogi, C., Ott, E., Yorke, J.A., Yorke, E.D., 1988. Multiple coexisting attractors, basin boundaries and basic sets. Physica D 32 (2), 296–305.

Belenky, V., 1993. A capsizing probability computation method. J. Ship Res. 37 (3), 200–207.

Belenky, V., 2000. Piecewise linear approach to nonlinear ship dynamics. In: Vassalos, D., Hamamoto, M., Papanikolaou, A., Molyneux, D. (Eds.), Contemporary Ideas on Ship Stability. Elsevier, pp. 149–160.

Belenky, V., Glotzer, D., Pipiras, V., Sapsis, T., 2019. Distribution tail structure and extreme value analysis of constrained piecewise linear oscillators. Probab. Eng. Mech. 57, 1–13.

Belenky, V., Sevastianov, N., 2007. Stability and Safety of Ships: Risk of Capsizing. Society of Naval Architects and Marine Engineers.

Belenky, V., Weems, K.M., Lin, W.M., 2008. Numerical procedure for evaluation of capsizing probability with split time method. In: Proceedings of the 27th Symposium on Naval Hydrodynamics. Seoul, Korea.

Belenky, V., Weems, K.M., Lin, W.M., 2016. Split-time method for estimation of probability of capsizing caused by pure loss of stability. Ocean Eng. 122, 333–343.
Belenky, V., Weems, K., Lin, W.-M., Pipiras, V., Sapsis, T., 2023. Estimation of probability of capsizing with split-time method. Ocean Eng. 292, 116452.
Belenky, V., Weems, K.M., Pipiras, V., 2018a. Extreme-value properties of the split-time metric. In: Proceedings of the 13th International Conference on the Stability of Ships and Ocean Vehicles. Kobe, Japan.
Belenky, V., Weems, K.M., Pipiras, V., Glotzer, D., Sapsis, T., 2018b. Tail structure of roll and metric of capsizing in irregular waves. In: Proceedings of the 32nd Symposium on Naval Hydrodynamics. Hamburg, Germany.
Belenky, V., Weems, K.M., Spyrou, K., Pipiras, V., Sapsis, T., 2017. Modeling broaching-to and capsizing with extreme value theory. In: Proceedings of the 16th International Ship Stability Workshop. Belgrade, Serbia.
Coles, S., 2001. An Introduction To Statistical Modeling of Extreme Values. Springer Series in Statistics, Springer-Verlag London Ltd..
Datseris, G., Wagemakers, A., 2022. Effortless estimation of basins of attraction. Chaos 32 (2), 023104.
Diebolt, J., Gardes, L., Girard, S., Guillou, A., 2008. Bias-reduced estimators of the Weibull tail-coefficient. Test 17 (2), 311–331.
Ekanayake, S.T., Cruise, J.F., 1993. Comparisons of Weibull-and exponential-based partial duration stochastic flood models. Stoch. Hydrol. Hydraul. 7 (4), 283–297.
Gardes, L., Girard, S., 2005. Estimating extreme quantiles of Weibull tail distributions. Comm. Statist. Theory Methods 34 (5), 1065–1080.
Gardes, L., Girard, S., 2006. Comparison of Weibull tail-coefficient estimators. Revstat 4 (2), 163–188.
Gardes, L., Girard, S., Guillou, A., 2011. Weibull tail-distributions revisited: a new look at some tail estimators. J. Statist. Plann. Inference 141 (1), 429–444.
Gitterman, M., 2005. The Noisy Oscillator: The First Hundred Years, from Einstein Until now. World Scientific.
Glotzer, D., Pipiras, V., Belenky, V., Campbell, B., Smith, T., 2017. Confidence intervals for exceedance probabilities with application to extreme ship motions. REVSTAT 15 (4), 537–563.
Gomes, M.I., Guillou, A., 2015. Extreme value theory and statistics of univariate extremes: a review. Internat. Statist. Rev. 83 (2), 263–292.
Hayashi, C., 2014. Nonlinear Oscillations in Physical Systems. Princeton University Press.
Lindgren, G., 2013. Stationary Stochastic Processes. Chapman & Hall/CRC Texts in Statistical Science Series, CRC Press, Theory and applications.
Madsen, H., Rosbjerg, D., Harremoës, P., 1993. Application of the partial duration series approach in the analysis of extreme rainfalls. In: Proceedings of the Yokohama Symposium. The International Association of Hydrological Sciences.
Mager, J., 2015. Automatic Threshold Selection of the Peaks Over Threshold Method (Master's thesis). The Technical University of Munich.
Mercadier, C., Soulier, P., 2012. Optimal rates of convergence in the Weibull model based on kernel-type estimators. Statist. Probab. Lett. 82 (3), 548–556.
Mohamad, M.A., Sapsis, T.P., 2015. Probabilistic description of extreme events in intermittently unstable dynamical systems excited by correlated stochastic processes. SIAM/ASA J. Uncertain. Quantif. 3 (1), 709–736.
Najafi, E., Babuška, R., Lopes, G.A.D., 2016. A fast sampling method for estimating the domain of attraction. Nonlinear Dyn. 86, 823–834.
Nayfeh, A.H., Mook, D.T., 2008. Nonlinear Oscillations. John Wiley & Sons.
Neves, C., Fraga Alves, M.I., 2004. Reiss and Thomas' automatic selection of the number of extremes. Comput. Statist. Data Anal. 47 (4), 689–704.
Pickands, J., 1975. Statistical inference using extreme order statistics. Ann. Statist. 3, 119–131.
Rosbjerg, D., Madsen, H., Rasmussen, P.F., 1992. Prediction in partial duration series with generalized Pareto-distributed exceedances. Water Resour. Res. 28 (11), 3001–3010.
Small, C.G., 2010. Expansions and Asymptotics for Statistics. CRC Press.
Sobczyk, K., 1991. Stochastic Differential Equations. Kluwer Academic Publishers, Dordrecht, The Netherlands.
Sólnes, J., 1997. Stochastic Processes and Random Vibrations: Theory and Practice. Wiley.
Spineili, J., Stephens, M.A., 1987. Tests for exponentiality when origin and scale parameters are unknown. Technometrics 29 (4), 471–476.
Stender, M., Hoffmann, N., 2022. bSTAB: an open-source software for computing the basin stability of multi-stable dynamical systems. Nonlinear Dynam. 107 (2), 1451–1468.
Timm, N.H., 2002. Applied Multivariate Analysis. Springer.
Todorovic, P., Zelenhasic, E., 1970. A stochastic model for flood analysis. Water Resour. Res. 6 (6), 1641–1648.